Sensitivity of downward longwave surface radiation to moisture and cloud changes in a high-elevation region

Catherine M. Naud,[1] Yonghua Chen,[1] Imtiaz Rangwala,[2,3] and James R. Miller[2]

Received 22 February 2013; revised 6 June 2013; accepted 9 July 2013.

[1] Several studies have suggested enhanced rates of warming in high-elevation regions since the latter half of the twentieth century. One of the potential reasons why enhanced rates of warming might occur at high elevations is the nonlinear relationship between downward longwave radiation (DLR) and specific humidity (q). Using ground-based observations at a high-elevation site in southwestern Colorado and coincident satellite-borne cloud retrievals, the sensitivity of DLR to changes in q and cloud properties is examined and quantified using a neural network method. It is also used to explore how the sensitivity of DLR to q (dDLR/dq) is affected by cloud properties. When binned by season, dDLR/dq is maximum in winter and minimum in summer for both clear and cloudy skies. However, the cloudy-sky sensitivities are smaller, primarily because (1) for both clear and cloudy skies dDLR/dq is proportional to 1/q, for $q > 0.5\ g\,kg^{-1}$, and (2) the seasonal values of q are on average larger in the cloudy-sky cases than in clear-sky cases. For a given value of q, dDLR/dq is slightly reduced in the presence of clouds and this reduction increases as q increases. In addition, DLR is found to be more sensitive to changes in cloud fraction when cloud fraction is large. In the limit of overcast skies, DLR sensitivity to optical thickness decreases as clouds become more opaque. These results are based on only one high-elevation site, so the conclusions here need to be tested at other high-elevation locations.

Citation: Naud, C. M., Y. Chen, I. Rangwala, and J. R. Miller (2013), Sensitivity of downward longwave surface radiation to moisture and cloud changes in a high-elevation region, *J. Geophys. Res. Atmos.*, *118*, doi:10.1002/jgrd.50644.

1. Introduction

[2] Mountain systems are critical to people and ecosystems, and they play a significant role as "water towers" within the terrestrial system. More than half of the global rivers have their origins in mountains, and since midlatitude to high-latitude rivers are often dominated by snowmelt runoff, it is important to understand how climate is changing in these environments in response to increasing levels of atmospheric greenhouse gases [*Christensen et al*., 2007].

[3] Since the latter half of the twentieth century, several high-elevation regions may be experiencing a greater rate of warming than low-lying areas at the same latitude, and the reason is still unclear [*Rangwala and Miller*, 2012 and references therein]. A number of positive feedbacks may be more active in these cold and dry regions, and the water vapor feedback may be one of the most potent [*Rangwala and Miller*, 2009; *Rangwala*, 2012]. One of the difficulties in assessing these feedbacks is the sparsity of observations in mountainous regions where radiation and cloud measurements are often missing. Several studies have already examined the nonlinear relationship between humidity and downward longwave radiation (DLR): the drier the atmosphere, the greater the impact of a small change in humidity on DLR [e.g., *Ruckstuhl et al.*, 2007; *Rangwala et al*., 2010; *Naud et al*., 2012]. However, it is unclear how clouds may affect this sensitivity, i.e., if clouds are present, is the impact of a change in moisture on DLR reduced?

[4] Using 6 years of ground-based observations of DLR and specific humidity (q) collected at a high-elevation site (3719 m altitude) in Colorado's San Juan Mountains, and coincident NASA Terra and Aqua Moderate resolution Imaging Spectroradiometer (MODIS) [*Salomonson et al*., 1989] cloud fraction and optical thickness retrievals, we evaluate the impact of clouds on the DLR-q relationship. We not only explore the change in sensitivity of DLR to changes in q, as a function of q, when clouds are present but also the impact of changes in cloud fraction and optical thickness.

[5] For this, we use a neural network (NN) method as an alternative statistical method to traditional regression techniques; it has been widely used in environmental sciences and water resources since the 1990s. A neural network is a mapping model that relates one or several input variables to an output variable in a nonlinear way. In his review paper, *Stephens* [2005] recommends extending the classical feedback diagnostics to investigate instantaneous sensitivities

[1]Department of Applied Physics and Applied Mathematics, Columbia University, New York, New York, USA.
[2]Institute of Marine and Coastal Science, Rutgers, State University of New Jersey, New Brunswick, New Jersey, USA.
[3]Western Water Assessment, PSD NOAA ESRL, Boulder, Colorado, USA.

Corresponding author: C. M. Naud, Columbia University, 2880 Broadway, New York, NY 10025, USA. (cn2140@columbia.edu)

2169-897X/13/10.1002/jgrd.50644

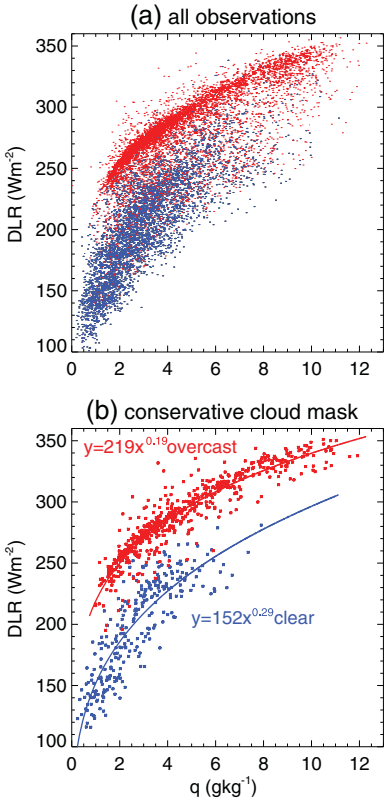

Figure 1. Daytime Senator Beck observations of downward longwave radiation (DLR) versus specific humidity (q), for clear (blue) and cloudy sky (red), using (a) all ground-based observations and (b) ground-based observations where the ground-based cloud mask and MODIS cloud fraction of exactly 0 and 100% (overcast) agree. The equations represent a least square fit (solid lines).

instead of equilibrium estimates. These sensitivities constitute a step toward a more realistic representation and evaluation of feedback processes, particularly in their time evolution and their roles in governing cloud-radiation interactions. Stephens suggests that the *Aires and Rossow* [2003] method is one way to obtain the instantaneous sensitivities, that is, to apply a neural network approach and examine the NN Jacobians.

[6] The Jacobian matrix contains the first partial derivatives of a given output variable with respect to a given input variable. This, by definition, is the sensitivity of the output variable to all input variables as inferred by the NN model. The neural network Jacobians can provide not only an estimate of the mean sensitivity between two variables but also an estimate of the distribution of the sensitivity. The advantage of this NN Jacobian is that it gives a direct statistical evaluation of the multivariate and nonlinear sensitivities that depends on each configuration of input and output variables [*Aires and Rossow*, 2003]. Consequently, we examine not only the NN outputs but also the Jacobian matrix within the neural network following the method of *Aires and Rossow* [2003]. Here, the input variables are specific humidity and either cloud fraction or cloud optical thickness, and the output variable is DLR.

2. Data

[7] We use two different sets of data, one obtained from a ground-based station and the other from a satellite. Both are described below.

2.1. Senator Beck Study Plot

[8] The Center for Snow and Avalanche Studies (www.snowstudies.org) installed and manages four different measurement stations within the Senator Beck Basin in southwestern Colorado. For our study, we choose one of these sites, the Senator Beck Study Plot (37.9°N–107.725°W, altitude 3719 m), because it is above tree line in an alpine tundra environment and exposed to strong winds that prevent cold air pooling issues as well as snow accumulation on the instruments. More detail on the site and instrumentation can be found in *Painter et al.* [2012]. Automated observations of temperature, relative humidity, and downward longwave and shortwave radiation (DLR and DSR), to only cite those used here, are performed every 5 s and provided as hourly averages, using the end of the hour as the reporting time (e.g., the 9 A.M. observation includes all 5 s intervals between 8 A.M. and 9 A.M.). The air temperature and relative humidity are measured with a Campbell-Vaisala CS500-U Humitter® and the radiation with a Kipp and Zonen CG4 180° field-of-view pyrgeometer for longwave and Kipp and Zonen CM21 for shortwave. The instruments are leveled in situ, at the top of a tower; slight shifts may occur after the operator gets off of the tower.

[9] The radiometers were installed with the original manufacturer's calibration and have gone through regular intervals of calibration by AccuFlux per Annex A.3.1 of the ISO-9847 Standard. Detailed information on the radiometers, including their calibration and other history can be found at http://snowstudies.org/data/metadata/SBSP_metadata.pdf. The radiometers are sufficiently ventilated owing to strong winds at the study site. There have only been rare instances of snow accumulation on the sensors (Landry, 2013, private communication). The pyrgeometer includes a solar blind filter that blocks all solar radiation. The solar radiation absorbed by the silicon window covering the radiometer is conducted effectively to facilitate very low heating effects even in full sunlight and allows for accurate daytime measurements without the need for a shading disc. Both instruments are expected to have an accuracy well within 2%, and as we explore sensitivities, i.e., differences in fluxes, we do not expect biases large enough to affect our conclusions.

Table 1. Daytime Seasonal Average of Sensitivity of Downward Longwave Radiation DLR to Specific Humidity q (dDLR/dq) and Specific Humidity (q) for Clear and Cloudy Sky, When Both Cloud Masks Agree

	Clear Sky		Cloudy Sky	
Season	q ($g\,kg^{-1}$)	dDLR/dq ($Wm^{-2}(g\,kg^{-1})^{-1}$)	q ($g\,kg^{-1}$)	dDLR/dq ($Wm^{-2}(g\,kg^{-1})^{-1}$)
Winter	1.3	36	2.8	18
Spring	2.0	27	3.6	15
Summer	3.9	17	7.7	8
Autumn	3.2	19	4.9	11

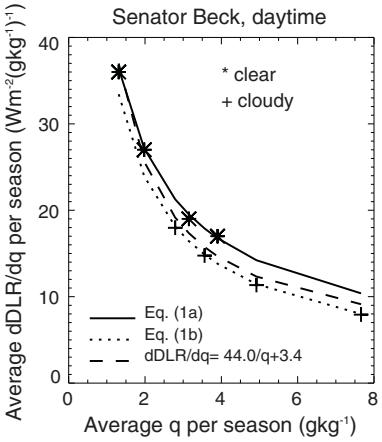

Figure 2. Seasonal average of dDLR/dq as a function of average q for clear- (star) and cloudy- (cross) sky observations as presented in Table 1. The dashed line represents a linear fit of both cloudy and clear-sky points as a function of 1/q, while the solid line represents the first derivative of equation (1a) and the dotted line the first derivative of equation (1b).

[10] For surface air pressure, we use measurements from the nearby Swamp Angel Study Plot (37.9°N–107.711°W; 3371 m) and estimate them for Senator Beck Study Plot using a linear relationship of pressure with elevation. Although, air pressure changes exponentially with elevation along the atmospheric column, the assumption of a linear relationship is valid for small elevation differences (here < 350 m). We use the surface air pressure, along with relative humidity and temperature to calculate the specific humidity (q). We also estimated surface air pressure at the study site using a hypsometric equation. The difference in calculation of q from the two different pressure estimates is less than 6%.

[11] The hourly DLR, DSR, and q data are available from 2005 onward, but here we selected data over 6 years from the beginning of the collection. This gave a total of 58,517 valid hourly observations of which 31,322 occurred during daytime.

2.2. MODIS

[12] The moderate resolution imaging spectroradiometer (MODIS) is mounted on both NASA Terra and Aqua platforms and observes the Earth with 36 channels at wavelengths between 0.4 and 14 μm since 1999 and 2002 respectively. The MODIS cloud retrievals are described in *Platnick et al*. [2003] and are archived in the MOD06 and MYD06 files for Terra and Aqua platforms, respectively. Here we collect from both platforms the 5 min long granules that overpass the Senator Beck station. This can occur 2–3 times a day, depending on the orbits. Only MODIS 5 km pixels that contain the ground site are used here. Cloud fractions (CF) are calculated from the 1 km cloud mask [*Platnick et al*., 2003; *Ackerman et al*., 2008], and thus vary between 0 and 100% in 4% increments. Cloud optical thicknesses (τ) are available at 1 km, but here we only use the central pixel in a 5×5 km zone to match the cloud fraction resolution. These retrievals are only performed during the daytime hours, because visible channels are used and only on pixels with a near complete cloud fraction to avoid retrieval errors caused by clear-sky contamination.

[13] Uncertainties in the MODIS cloud mask are described in *Ackerman et al*. [2008]. Clouds are missed when their optical thickness is less than 0.4 and also in polar regions at night. However, daytime observations in these regions with bright surfaces were found to be mislabeled only 5% of the time. We anticipate issues with the MODIS cloud fractions in high-elevation regions to be largest in the winter when snow is present, at night, and when thin cirrus are present. Consequently, some of the clear-sky points in our data set may in fact contain clouds. For overcast scenes and optical thicknesses greater than 0.4, the MODIS optical thicknesses are expected to be of good quality [e.g., *Painemal and Zuidema*, 2011].

[14] To relate cloud observations with the ground measurements of q and DLR, we require the MODIS observing time to be within the hour reported in the ground-based measurements. This reduces the daytime ground-based data set with coincident cloud fraction to 3975 hourly observations. The data set is further reduced to 1491 hourly observations when we examine cloud optical thickness because it is only available for mostly overcast 1 km pixels.

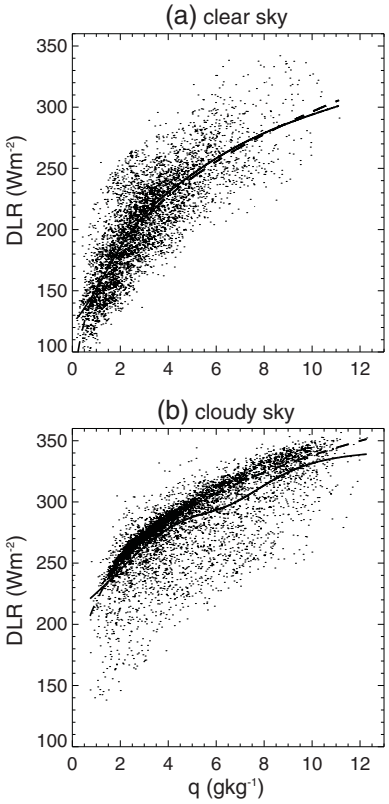

Figure 3. Downward longwave radiation (DLR) as a function of specific humidity (q) for all (a) clear-sky and (b) cloudy-sky points processed by the neural network. The solid line shows the fit estimated by the neural network and the dashed line the fits given in equations (1a) for clear sky and (1b) for overcast sky.

Table 2. Average Per NN Bin (From Low to High Sensitivity) of Clear Sky and Cloudy Sky[a]

	Clear Sky: Average Per Bin					Cloudy Sky: Average Per Bin				
NN Bins: Low to High dDLR/dq	N	dDLR/dq (Wm^{-2} $(g\,kg^{-1})^{-1}$)	DLR (Wm^{-2})	q ($g\,kg^{-1}$)	T (°C)	N	dDLR/dq (Wm^{-2} $(g\,kg^{-1})^{-1}$)	DLR (Wm^{-2})	q ($g\,kg^{-1}$)	T (°C)
1	552	11 (2)	267	6.7	10.8	634	5.4 (1)	301	6.9	4.7
2	1408	16 (2)	228	4.1	8.0	1530	8.4 (1)	301	6.5	3.9
3	826	24 (2)	207	2.7	3.3	1397	12.4 (1)	290	5.5	1.6
4	1909	32 (2)	171	1.6	−4.7	2168	18.2 (1)	254	2.5	−8.6

[a]N (number of points per bin), dDLR/dq (sensitivity of downward longwave radiation DLR to specific humidity q) with associated one standard deviation per bin in parenthesis, downward longwave radiation (DLR), specific humidity (q), and T is the surface air temperature. Each bin is of equal range in dDLR/dq.

3. Methods

[15] In this section, we first describe how we delineate clear- and cloudy-sky conditions using a method based on ground-based observations of incident solar radiation and then describe the neural network technique.

3.1. Ground-Based Cloud Mask

[16] We use downward solar radiation measurements to determine clear- and cloudy-sky conditions on a diurnal basis using a strict criterion. For each month, if the daily mean solar radiation is one standard deviation above the monthly mean, we flag the whole diurnal period as a clear-sky case, and if the radiation is one standard deviation below the monthly mean, we flag it as a cloudy-sky case. All data points within the one standard deviation are excluded from the analysis, thereby reducing the ground-based daytime hourly data pool to 10,424 hourly observations.

[17] To assess the performance of this ground-based cloud mask, we perform a comparison with the MODIS observations. We require the measurements from the ground and satellite to be coincident within half an hour and define the MODIS cloud mask such as clear sky is for 0% cloud fraction and cloudy sky for 100% cloud fraction. We compare 931 daytime hourly observations and both platforms agree it was clear for 272 observations, agree it was cloudy for 629 observations and disagree for 30 observations. This implies a disagreement of only 3% between the two platforms during the daytime hours. Note that this disagreement increases to 22% for the night time hourly observations. These results give great confidence in the ground-based cloud mask for the daytime observations, and, therefore, only daytime observations are used for analysis in this study.

3.2. Neural Network

[18] The neural network (NN) approach is described briefly in this section. A much more detailed description, including an illustrative example, is given in *Chen et al.* [2006]. A neural network is a nonlinear mapping model that, given an input variable, provides an output quantity in a nonlinear way. In this paper the output variable is DLR and the input variables are specific humidity, cloud fraction, and cloud optical thickness.

[19] A by-product of a neural network model is the NN Jacobian matrix. This NN Jacobian matrix is equivalent to obtaining the first partial derivative of a given output variable with respect to a given input variable and will be a critical component of our analysis in this paper. These Jacobians have been used to add constraints in a radiative transfer model [e.g., *Aires et al*., 1999] for variational assimilation applications [*Chevallier and Mahfouf*, 2001] or to investigate sensitivities in a remote sensing algorithm [*Aires et al*., 2001]. In a different context, the NN Jacobians were integrated into a theoretical framework as a tool to study the instantaneous, multivariate, nonlinear sensitivities in climate feedback processes [*Aires and Rossow*, 2003]. *Chen et al.* [2006] presented a test case that showed that NN estimates could capture nonlinear relationships much better than the traditional linear regression method. In this paper we use the same NN model as *Chen et al*. [2006].

[20] Initially, about half of the data are randomly selected from the data set to train the neural network. The NN is optimized using the training data set, and the training process is stopped when the root mean square error between iterations is small [*Bishop*, 1996]. The neural network structure obtained after this process is referred to as a trained neural network. Since there is some concern about overtraining in the NN model, another portion of the original data set is used to perform an independent validation of the trained neural

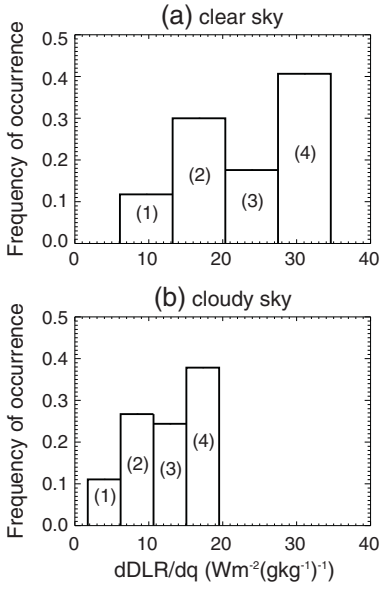

Figure 4. Frequency of occurrence of dDLR/dq sorted into four separate NN bins for (a) clear- and (b) cloudy-sky observations. The frequency of occurrence is defined as the ratio of number of points per bin to the total number of points in the data set. Each bin is of equal sensitivity range. See Table 2 for the average properties of each bin.

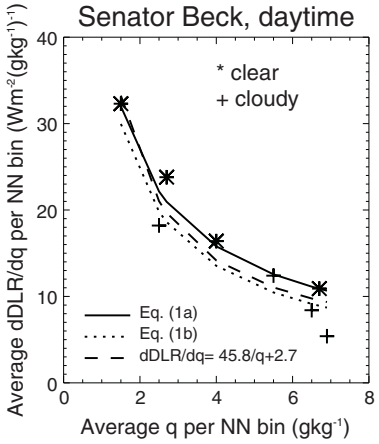

Figure 5. Average of dDLR/dq per NN bin as a function of average q for clear- (star) and cloudy- (cross) sky conditions as presented in Table 2. The dashed line is a linear fit in 1/q, the solid line is the first derivative of equation (1a), while the dotted line is the first derivative of equation (1b).

network. If the errors between the NN predictions and the validation data set are small, we assume there is no overtraining in the NN model, and that the NN is providing the correct output variables given the specified inputs. One limitation of the NN model is that it requires a large number of data points, generally a few thousand, but we do have enough for our analysis here.

[21] We apply the NN method to three sets of data: (1) the full set with only ground observations during the daytime hours using the ground-based cloud mask (10,424 data points, section 4.1), (2) the subset for which MODIS cloud fractions are available (3975 data points, section 4.2), and (3) the subset of data for which MODIS cloud optical thicknesses are available (1491 data points, section 4.3). In each case the output variable is DLR, and we are particularly interested in the Jacobian matrix that provides the sensitivity of DLR to changes in q and show how the sensitivities are affected by clouds. We consider both bivariate (one input variable) and multivariate (two input variables) cases. For the bivariate case discussed in section 4.1, the input variable is q. For the multivariate cases, the input variables are q and cloud fraction (section 4.2), and q and cloud optical thickness (section 4.3).

4. Results

[22] This section is divided into three parts. We first examine the sensitivity of DLR to changes in q separately for clear and cloudy skies, regardless of cloud properties. In the second section we examine the effect of changes in cloud fraction on the DLR-q sensitivities. In the last section we include a discussion of the effect of changes in cloud optical thickness (τ) on the sensitivities in overcast cases (cloud fractions of 100%). For all experiments, only daytime observations are used to avoid inclusion of erroneous cloud detections for both ground and satellite measurements.

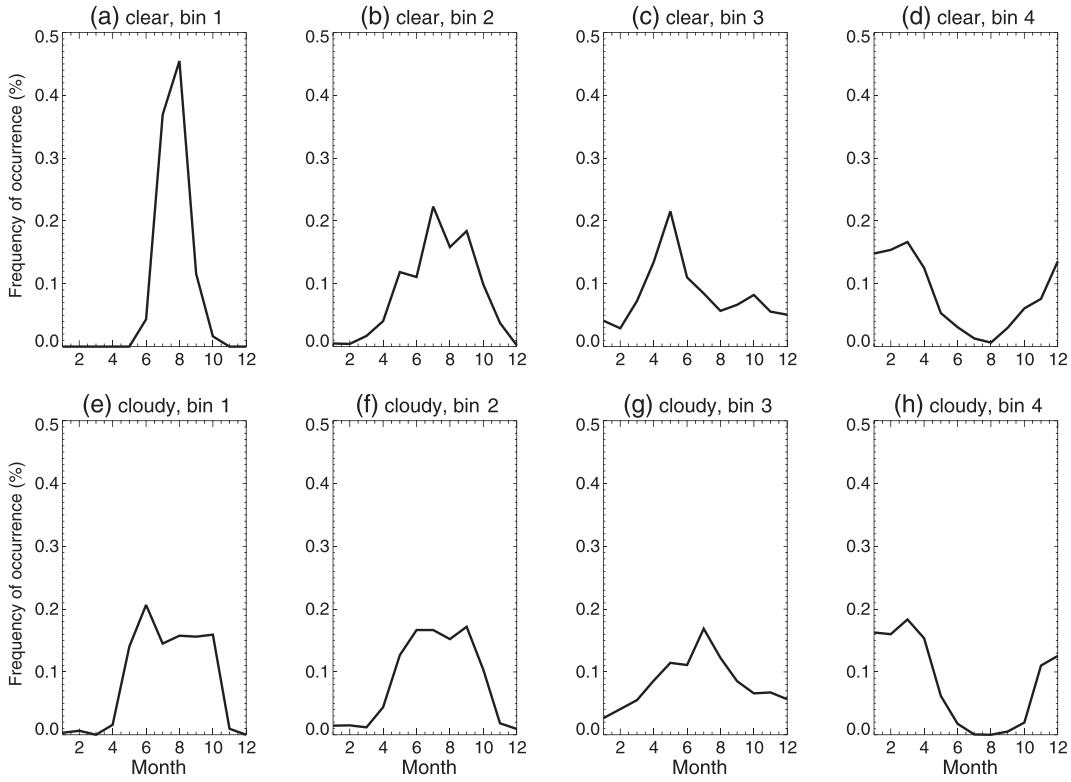

Figure 6. Frequency of occurrence of month per NN bin for (top) clear- and (bottom) cloudy-sky conditions (left to right) from low sensitivity (bin 1) to high sensitivity (bin 4). Each bin is of equal dDLR/dq range. The frequency of occurrence is defined as the ratio of number of points per month to the total number of points in the bin.

Table 3. Variable Correlation Matrix From NN Experiment With DLR as a Function of q and Cloud Fraction (CF)

Variable/Variable	DLR	q	CF
DLR	1.00	0.81	0.61
q	0.81	1.00	0.30
CF	0.61	0.30	1.00

4.1. DLR Sensitivity to Specific Humidity: Clear Versus Cloudy Sky

[23] We first use all of the hourly observations measured at the ground to examine the relationship between DLR and q, and we then apply the ground-based cloud mask to separate clear- from cloudy-sky cases. Figure 1a shows how the relationship between DLR and q changes when clouds are present. Two distinct clusters can be seen, with DLR larger for the cloudy-sky cluster as expected owing to the blackbody effect of the clouds on DLR. The clear-sky cluster exhibits a longer tail toward the lower values of q, while the cloudy-sky cluster reaches further into the higher values of q.

[24] Although two main clusters emerge as clear- and cloudy-sky observations are delineated, there are many observations that fall between these two main clusters. These points may be observations for which (1) the cloud mask is wrong, (2) the cloud fraction is small, or (3) the cloud optical thickness is low. In order to correct for problems 1 and 2, we enforce a strict selection criterion that only retains observations when both the ground-based and MODIS cloud masks (defined as clear sky for 0% cloud fraction and cloudy sky for 100%) agree. For this subset, Figure 1b shows a better separation between clear- and overcast- (100% cloud fraction) sky observations, with overcast-sky DLR values being larger for a given q, and clear-sky values of q extending to lower values. We evaluate the relationship between DLR and q separately for clear- and overcast-sky conditions by applying a regression fit to the log of DLR and q and obtain

$$\mathrm{DLR} = 152\, q^{0.29} \text{ for clear sky} \quad (1a)$$

$$\mathrm{DLR} = 219\, q^{0.19} \text{ for overcast sky} \quad (1b)$$

[25] A first order derivative of both fits indicates that the sensitivities at low values of q are slightly lower in overcast conditions (e.g., for $q = 2\ \mathrm{g\,kg^{-1}}$, $\mathrm{dDLR/dq} = 27\ \mathrm{Wm^{-2}\ (g\,kg^{-1})^{-1}}$ for clear sky and $23\ \mathrm{Wm^{-2}\ (g\,kg^{-1})^{-1}}$ for cloudy sky).

[26] Table 1 shows the average seasonal dDLR/dq sensitivities calculated from the slopes of the power law curves shown in Figure 1b at mean seasonal q values associated with both the clear- and overcast-sky cases. For both conditions, sensitivities are largest in the winter, and lowest in summer, but sensitivities are much lower for overcast sky. This is because the average seasonal q is larger when clouds are present, causing the sensitivities to decrease. By plotting the relation between average sensitivity and average q as given in Table 1, we examine whether for a given q, the sensitivities change between clear- and cloudy-sky conditions. Figure 2 indicates the sensitivity is only slightly lower in the presence of clouds (when overcast), although the two fits obtained from equation (1) suggest this decrease in sensitivity increases with increasing q. However, uncertainty in observations and method prevent any definite conclusion as to the actual impact of clouds. A least square regression assuming a linear relationship between the sensitivity and 1/q also provides a reasonable fit to both clear- and cloudy-sky conditions, in between the first derivatives of equations (1a) and (1b).

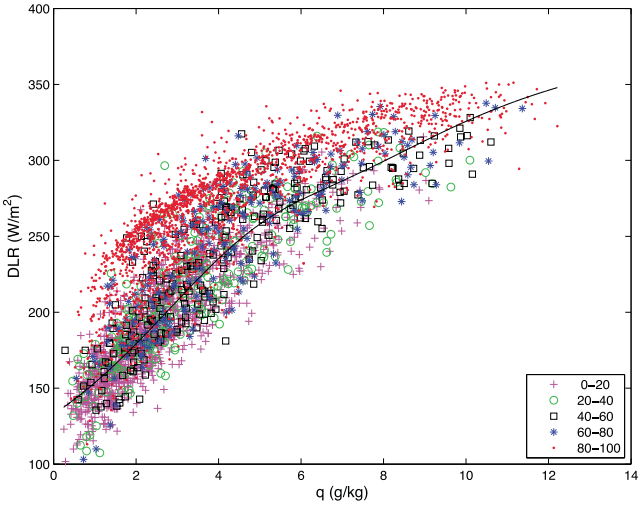

Figure 7. Downward longwave radiation (DLR) as a function of specific humidity (q) for all cloudy-sky cases (cloud fractions from 0 to 100%), with different symbols per cloud fraction range: magenta cross for 0 to 20%, green circle for 20–40%, black square for 40–60%, blue star for 60–80%, and red dot for 80–100%. The solid line shows the overall fit found by the neural network.

[27] We next use the NN to process all observations (regardless of the value of the MODIS cloud fraction, as in Figure 1a) separately for clear- and cloudy-sky conditions (determined with the ground-based cloud mask). This allows

Table 4. Average Properties of Each NN Bin of ∂DLR/∂q for All Cloud and Clear-Sky Cases (Cloud Fraction (CF) From 0 to 100%)[a]

NN Bins: Low to High ∂DLR/∂q	N	∂DLR/∂q	DLR	q	T	CF	∂DLR/∂CF	τ
		$(\mathrm{Wm^{-2}(g\,kg^{-1})^{-1}})^{-1}$	$(\mathrm{Wm^{-2}})$	$(\mathrm{g\,kg^{-1}})$	(°C)	(%)	$(\mathrm{Wm^{-2}(\%)^{-1}})$	(Unitless)
1	798	8	307	7.5	9.1	82	0.5	26
2	383	15	275	4.9	5.5	72	0.5	27
3	1376	22	242	2.9	−2.4	81	0.8	22
4	1418	27	192	2.2	−0.1	25	0.1	20

[a]Each bin is of equal ∂DLR/∂q range.

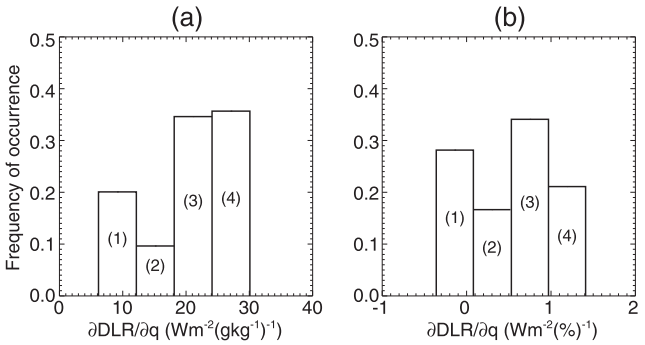

Figure 8. Frequency of occurrence of (a) ∂DLR/∂q and (b) ∂DLR/∂CF sorted into four NN bins where CF is cloud fraction. The frequency of occurrence is defined as the ratio of number of points per bin to the total number of points in the data set. Each bin is of equal sensitivity range. See Table 4 for average properties of each bin in Figure 8a and Table 5 for Figure 8b.

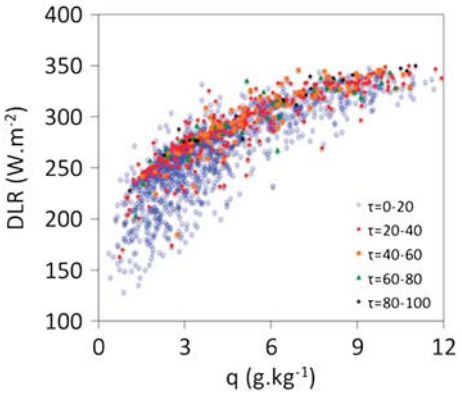

Figure 9. Downward longwave radiation (DLR) as a function of specific humidity (q) for cloudy-sky conditions, with different colors for different cloud optical thicknesses τ: 0–20 (blue), 20–40 (red), 40–60 (orange), 60–80 (green), and 80–100 (black).

us to verify if the results from the NN method are consistent with the least square regression method used above, and further helps in their interpretation. Figure 3a shows a scatter plot of DLR versus q for all points used in the neural network for clear sky only, while Figure 3b shows the cloudy-sky case. The solid line represents a fit automatically generated by the NN, while the dashed lines show the fits given by equations (1a) and (1b). For clear-sky conditions, the NN method gives a fit very similar to the one found for the restricted data set in Figure 1b. For cloudy-sky cases, the correspondence between equation (1b) and the NN fit is fairly good for $q < 4$ g kg^{-1} but there is more deviation for larger values of q. Part of this bias would arise from the fact that for the NN fit all cloudy points are included, while equation (1b) is only for strictly overcast cases. This suggests the inclusion of cloud fractions less than 100% has a larger impact on the DLR-q relationship for larger values of q. In addition, the number of observations decreases rapidly with q for $q > 4$ g kg^{-1}, which may also affect the quality of both fits.

[28] The NN results are then binned according to specified criteria, e.g., month, sensitivity, cloud fraction, q, and cloud optical thickness. We sort the results by sensitivity into four bins with equal sensitivity range for each bin. If one desires higher resolution of the sensitivities, then more bins can be specified. Since the ranges of sensitivities in each of the four bins are equal, there is no expectation that each bin will contain the same number of observations, and Table 2 shows that to be the case. Table 2 also includes the mean quantities for each bin and the standard deviation of the sensitivities per bin. Figure 4 shows the frequency of occurrence of the DLR-q sensitivities sorted into these four separate bins for both clear- and cloudy-sky conditions. For both clear- and cloudy-sky conditions, the lowest sensitivity bin is the least populated while the highest sensitivity bin is the most populated. For all four sensitivity bins, cloudy-sky conditions exhibit lower sensitivities than clear-sky conditions. When exploring the relationship between the average sensitivity and average q per bin (Table 2), for both clear- and cloudy-sky conditions, Figure 5 shows that we obtain a linear fit in 1/q that is very close to the seasonal relationship shown in Figure 2. However, there is more scatter in the cloudy-sky points (cf. Figure 3b), and it becomes difficult to reconcile the overcast sky fit of equation (1b) (dotted line) with the cloudy-sky points in Figure 5 at the lower sensitivity—larger q end.

[29] We next examine the temporal distribution of each of the four bins in Figure 4 by separating the sensitivities by month for both clear- and cloudy-sky conditions. Figure 6 reveals that the lowest sensitivity bin (bin 1) contains mostly summer months, for both clear- and cloudy-sky conditions, although for cloudy conditions, late spring and early fall are also represented. The second bin includes, in both cases, late spring, summer, and early fall. For the third bin, the distribution is slightly different between clear- and cloudy-sky conditions, with most months represented for both, but with a peak in late spring for clear-sky cases and a peak in summer for cloudy-sky cases. Finally, the highest sensitivity bin (bin 4) occurs in winter and early spring for both clear- and cloudy-sky conditions. Compared with the sensitivities

Table 5. Same as Table 4 but for Bins of Equal ∂DLR/∂CF Range

NN Bins: Low to High ∂DLR/∂CF	N	∂DLR/∂CF	DLR	q	T	CF	∂DLR/∂q	τ
		(Wm^{-2}(%)$^{-1}$)	(Wm^{-2})	(g kg^{-1})	(°C)	(%)	(Wm^{-2}(g kg^{-1})$^{-1}$)	(Unitless)
1	1119	−0.2	187	2.2	1.6	4	25	NA
2	662	0.3	264	5.9	8.2	45	16	27
3	1355	0.7	278	5.0	3.3	92	16	24
4	839	1.1	232	2.1	−7.0	97	24	22

Table 6. Variable Correlation Matrix From NN Experiment With DLR as a Function of q and Cloud Optical Thickness τ

Variable/Variable	DLR	q	τ
DLR	1.00	0.85	0.21
q	0.85	1.00	0.10
τ	0.21	0.10	1.00

given in Table 1 where seasons are intentionally separated, the lowest and highest sensitivity bins obtained with the NN strongly resemble the summer and winter sensitivities, respectively.

[30] Using both the NN and a direct method, we find that the sensitivity of DLR to changes in q is similar whether clouds are present or not, albeit with a slight reduction in cloudy-sky DLR-q sensitivities for a given q. In this section, our focus has been on clear- and cloudy-sky conditions regardless of cloud properties; we next investigate the impact of changing cloud fraction.

4.2. DLR Sensitivity to Specific Humidity and Cloud Fraction

[31] We now use the neural network to investigate sensitivities of DLR to both changes in q and cloud fraction. This experiment is conducted on the subset for which MODIS cloud fractions are available (3975 data points). The NN variable correlation matrix (Table 3) indicates a stronger correlation between DLR and q than between DLR and cloud fraction. Also, it shows that the correlation between q and cloud fraction is low.

[32] Figure 7 shows the relationship between DLR and q for all points with cloud fractions between 0 (clear sky) and 100% (overcast). It also shows how this relationship changes with cloud fraction and how most observations with a cloud fraction less than 80% fall onto the clear-sky cluster while fractions greater than 80% tend to follow the overcast cluster (see Figure 1b). The all-points NN fit tends to be closer to the clear-sky/low cloud fraction cluster than the overcast cluster.

[33] For the two-variable experiment with changes in q and CF, the NN output is first partitioned into four distinct bins of equal ∂DLR/∂q range for all observations including those with intermediate cloud fraction, clear, and overcast skies. Table 4 gives the average properties for each bin, and Figure 8a shows the frequency of occurrence of the ∂DLR/∂q bins. The distribution of sensitivities differs slightly from purely clear- or overcast-sky cases (see Figure 4). The sensitivities in each bin lie between those in the clear- and cloudy-sky bins, and we find that they align with the 1/q fit in Figure 5 (not shown). Focusing on the two highest sensitivity bins, 3 and 4, we find that their properties are very different (Table 4). For bin 3, the cloud fractions are large (around 80% on average), while for bin 4, the cloud fractions are low (around 25%). Also, the sensitivity of DLR to changes in cloud fraction in bin 3 is much larger than in bin 4. Finally, bin 3 is colder with slightly larger mean specific humidity than bin 4. Thus, for similar DLR-q sensitivities (22 versus 27 $Wm^{-2}(g\,kg^{-1})^{-1}$ for bins 3 and 4, respectively), and fairly close values of q (2.9 versus 2.2 $g\,kg^{-1}$), the bin with high cloud fractions exhibits sensitivities of DLR to q of the same order as the bin with the low cloud fractions. This suggests that cloud fraction has a minor impact on the sensitivity of DLR to q, at least for q between 2 and 3 $g\,kg^{-1}$.

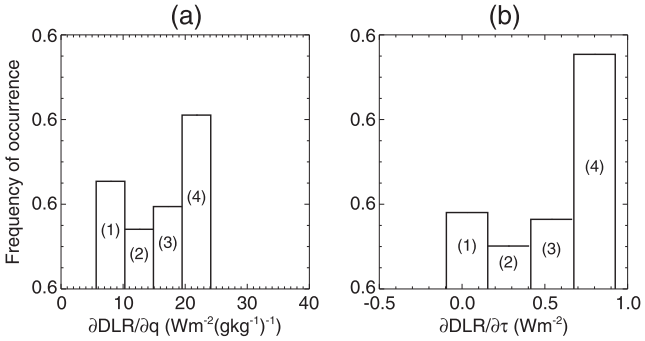

Figure 10. Frequency of occurrence of (a) ∂DLR/∂q and (b) ∂DLR/∂τ sorted into four NN bins. The frequency of occurrence is defined as the ratio of number of points per bin to the total number of points in the data set. Each bin is of equal sensitivity range. See Table 7 for the average properties of each bin in Figure 10a and Table 8 for Figure 10b.

[34] We now examine the same outputs but this time partitioned into four bins of equal sensitivity to cloud fraction. This differs from the discussion in the previous paragraph because the binning is now performed according to the sensitivities of DLR to changes in cloud fraction rather than to changes in q. Table 5 summarizes the average properties of each bin, and Figure 8b shows the frequency of occurrence of each bin. The distribution displays fewer high sensitivity points as compared to other distributions that have been shown. Table 5 shows that cloud fraction is positively correlated with DLR-CF sensitivities, i.e., higher values of cloud fraction associated with higher values of DLR-CF sensitivities. The lowest and highest DLR-CF sensitivity bins also correspond to cases with low specific humidity (2.2 versus 2.1 $g\,kg^{-1}$) and high DLR-q sensitivities (25

Table 7. Same as Table 4 for Data Set With Overcast Clouds and Cloud Optical Thickness (τ) Retrievals[a]

NN Bins: Low to High ∂DLR/∂q	N	∂DLR/∂q	DLR	q	T	∂DLR/∂τ	τ
		$(Wm^{-2}(g\,kg^{-1})^{-1})$	(Wm^{-2})	$(g\,kg^{-1})$	(°C)	(Wm^{-2})	(Unitless)
1	379	8	320	7.8	7.9	0.4	29
2	210	13	292	5.0	2.3	0.5	28
3	290	17	271	3.6	−2.3	0.5	28
4	612	22	243	2.3	−7.5	0.7	19

[a]Each bin is of equal ∂DLR/∂q range.

Table 8. Same as Table 7 but for Bins of Equal $\partial DLR/\partial\tau$ Range

NN Bins: Low to High $\partial DLR/\partial\tau$	N	$\partial DLR/\partial\tau$	DLR	q	T	τ	$\partial DLR/\partial q$
		(Wm^{-2})	(Wm^{-2})	($g\,kg^{-1}$)	(°C)	(Unitless)	($Wm^{-2}(g\,kg^{-1})^{-1}$)
1	269	−0.0	293	5.1	-1.0	75	13
2	151	0.3	294	5.3	0.1	31	14
3	245	0.6	290	5.1	0.3	20	14
4	826	0.8	261	3.7	−1.9	8	18

versus 24 $Wm^{-2}(g\,kg^{-1})^{-1}$). This means that, at low values of q (~2 $g\,kg^{-1}$) and high values of DLR-q sensitivities, when cloud fractions are low, DLR is marginally sensitive to changes in cloud fraction but when the cloud fraction is large, DLR is very sensitive to changes in cloud fraction. This suggests that at high cloud fraction, the $\partial DLR/\partial CF$ sensitivity does not saturate in the low q range. Next, we investigate the impact of cloud optical thickness during overcast conditions.

4.3. DLR Sensitivity to Specific Humidity and Cloud Optical Thickness

[35] As explained earlier, MODIS optical thickness retrievals are only performed during the daytime for pixels that are mostly overcast. Therefore, we can study the impact of changes in optical thickness without much interference from changes in cloud fraction. This means the subset of points used will be smaller than those described in section 4.2 (i.e., 1491 instead of 3975 data points). Figure 9 shows the relationship between DLR and q in overcast situations as a function of cloud optical thickness (color coded). The points are transitioning from the cloudy to clear-sky cluster as clouds become more transparent ($\tau < 20$). This is similar to the behavior we observed when cloud fraction decreased. Table 6 shows the variable matrix for this NN experiment, with DLR and q highly correlated while DLR and cloud optical thickness are weakly correlated.

[36] For this subset of points (overcast with an optical thickness retrieval available), we again partition the output data points into four equal range bins based on the values of $\partial DLR/\partial q$. The lowest DLR-q sensitivity bin exhibits the highest values of cloud optical thickness, while the highest sensitivity bin exhibits the lowest values of cloud optical thickness (Table 7). The neural network yields a bimodal distribution of sensitivities of DLR to q (Figure 10a), with the maximum occurrence for the lowest and highest sensitivity bins. In fact, Table 7 shows little change in optical thickness for bins one through three. This suggests that thicker clouds reduce the impact of q on DLR, while as clouds become more transparent, the impact of q on DLR increases.

[37] Then we partition the data points into four bins of equal $\partial DLR/\partial\tau$ range. The average properties of each bin are given in Table 8, and Figure 10b shows the distribution of sensitivity of DLR to cloud optical thickness in the four bins. There are two main modes of DLR sensitivities to changes in τ, one highly populated for the highest sensitivities and the second most populated mode is for the lowest sensitivity. We find that low DLR-τ sensitivities correspond to cases with high optical thickness and relatively large q (Table 8). Considering bins 1 to 3 where DLR, q, and $\partial DLR/\partial q$ are fairly similar, the DLR-τ sensitivity increases as the optical thickness decreases.

[38] These results suggest that in overcast situations, as optical thickness increases, sensitivity of DLR to τ decreases. Furthermore, for mean $\tau \geq 20$ (bins 1–3), $\partial DLR/\partial q$, and q remain more or less constant which suggests a saturation effect whereby the impact of changes in τ has less and less effect on DLR-q sensitivities once τ is above a certain value. However, $\partial DLR/\partial\tau$ and $\partial DLR/\partial q$ are largest for semitransparent clouds (mean $\tau = 8$).

5. Conclusions

[39] Using ground-based observations of DLR and q at one high-elevation location in southwestern Colorado, we investigate the relationship between these two variables, in cloud-free and cloudy conditions. Both a simple regression and a neural network method suggest that clouds not only increase DLR for a given q, they also slightly reduce the sensitivity of DLR to q, and this reduction increases with increasing q. Despite uncertainties in the measurements themselves and in the method that may affect the significance of these results, this reduction is consistent with previous work by *Ruckstuhl et al*. [2007]. They examined the sensitivity of DLR to q for clear- and all-sky conditions and found a slightly lower sensitivity in all-sky conditions.

[40] Overall, the sensitivity of DLR to changes in cloud fraction increases with cloud fraction. When the sky is overcast, DLR is sensitive to changes in optical thickness. However, as clouds become optically thicker, DLR reaches saturation and additional changes in DLR with cloud optical thickness are small. The sensitivity of DLR to changes in q is largest at low values of q, and in these conditions, cloud fraction changes have a minor impact on this sensitivity. However, for overcast clouds in fairly humid conditions, increases in optical thickness tend to decrease the DLR-q sensitivity.

[41] For each neural network experiment, we find that the highest sensitivities to changes in q are the following:

[42] 1. 32 $Wm^{-2}(g\,kg^{-1})^{-1}$ for $0 < q < 2$ $g\,kg^{-1}$ (clear sky);

[43] 2. 18 $Wm^{-2}(g\,kg^{-1})^{-1}$ for $1.5 < q < 3.5$ $g\,kg^{-1}$ (cloudy sky, 100% cloud fraction);

[44] 3. 27 $Wm^{-2}(g\,kg^{-1})^{-1}$ for $0 < q < 4$ $g\,kg^{-1}$ (all cloud fractions from 0 to 100% included); and

[45] 4. 22 $Wm^{-2}(g\,kg^{-1})^{-1}$ for $0 < q < 4$ $g\,kg^{-1}$ (cloudy sky, 100% fraction, optical thickness retrieved)

which means for a change in q of 2 $g\,kg^{-1}$, DLR changes by up to 65 Wm^{-2}, 36 Wm^{-2}, 54 Wm^{-2}, and 44 Wm^{-2}, respectively. The differences among these sensitivities are caused in part by different ranges of q within the highest sensitivity

bins. Potentially, the nighttime observations (not considered here) during winter or spring will have even drier and colder conditions, which will lead to realizations of even higher magnitudes of DLR-q sensitivities. Preliminary tests confirm this hypothesis, but issues with the cloud mask need to be resolved before any definite conclusion can be reached. We also note here that these changes in DLR are likely to be upper bounds on the response to changes in q because increases in temperature cause DLR to increase, and we have not considered the impact of changes in temperature which tend to be positively correlated with changes in q.

[46] Quantifying the influence of cloud properties on DLR, we find a DLR change of 0.8 Wm^{-2} per unit of optical thickness when optical thickness is between 0 and 20, and a DLR change of 1.1 $Wm^{-2}(\%)^{-1}$ for cloud fraction between 80 and 100%. These entail a maximum change in DLR of 16 Wm^{-2} for a 20 unit change in optical thickness, and a DLR change of 22 Wm^{-2} for a 20% change in cloud fraction. In general, we find the impact on DLR from a change in q, for the range of q available at this elevation, to be greater than that from a change in either cloud optical thickness or cloud fraction. Although these numbers are only indicative of what the real cloud effect might be, these results are qualitatively sound, as errors in the MODIS retrievals will mostly affect nighttime observations which are not used here. In addition, optically thin clouds, which are also a source of errors for MODIS retrievals, are not found to have a large impact. Furthermore, ground measurement uncertainties are small and suffer from no systematic bias, and are further reduced by using multiple years and a large sample.

[47] Overall, our experiments suggest the presence of clouds has a very limited influence on the sensitivity of DLR to q in the low q range ($<5\ g\,kg^{-1}$). However, at higher values of q, clouds tend to reduce this sensitivity. In the context of a future warming at high elevations, which may be accompanied by increases in the atmospheric moisture, winter and early spring may see a significant increase in DLR and possibly accelerated warming that could be partially offset by a change in cloud properties. These results are obtained using only one high-elevation site during daytime, but include a large sample size that should reduce the impact of measurement uncertainties and interannual variability (which was found to cause an uncertainty of no greater than 10% in the exponents of equation (1)). The low values of the standard deviations of the seasonal sensitivities provide additional evidence that the errors in sensitivities are small. Nevertheless, further work is needed to include nighttime observations and compare our results with other high-elevation locations.

[48] **Acknowledgments.** The Senator Beck Basin observations are provided by the Center for Snow and Avalanche Studies (http://www.snowstudies.org/). The MODIS cloud product (MOD06/MYD06) files are provided by the Level 1 and Atmospheric Archive Distribution System at the NASA Goddard Space Flight Center. We thank Filipe Aires for helpful discussions of the neural net analysis and Chris Landry for information and clarification related to instrumentation at the Senator Beck study site. We also thank three anonymous reviewers for significantly improving this manuscript. This work is funded by the NSF grants 1064281 and 1064326.

References

Ackerman, S. A., R. E. Holz, R. Frey, E. W. Eloranta, B. C. Maddux, and M. McGill (2008), Cloud detection with MODIS. Part II: Validation, *J. Atmos. Oceanic Technol.*, *25*, 1073–1086.

Aires, F., and W. B. Rossow (2003), Inferring instantaneous, multivariate and nonlinear sensitivities for the analysis of feedback processes in a dynamical system: The Lorenz model case study, *Quart. J. Roy. Meteorol. Soc.*, *129*, 239–275.

Aires, F., M. Schmitt, N. Scott, and A. Chedin (1999), The weight smoothing regularisation for MLP for resolving the input contribution's errors in functional interpolations, *IEEE Trans. Neural Networks*, *10*, 1502–1510.

Aires, F., C. Prigent, W. B. Rossow, and M. Rothstein (2001), A new neural network approach including first-guess for retrieval of atmospheric water vapor, cloud liquid water path, surface temperature and emissivities over land from satellite microwave observations, *J. Geophys. Res.*, *106*, 14887–14907.

Bishop, C. M. (1996), *Neural Networks for Pattern Recognition*, pp. 482, Oxford University Press, Oxford.

Chen, Y., F. Aires, J. A. Francis, and J. R. Miller (2006), Observed relationships between Arctic longwave cloud forcing and cloud parameters using a neural network, *J. Climate*, *19*, 4087–4104.

Chevallier, F., and J. F. Mahfouf (2001), Evaluation of the Jacobians of infrared radiation models for variational data assimilation, *J. Appl. Meteorol.*, *40*, 1445–1461.

Christensen, J. H., B. Hewitson, A. Busuioc, A. Chen, X. Gao, R. Held, R. Jones, R. K. Kolli, W. Kwon, and R. Laprise (2007), Regional climate projections, *Climate Change, 2007: The Physical Science Basis. Contribution of Working group I to the Fourth Assessment Report of the Intergovernmental Panel on Climate Change, University Press, Cambridge, Chapter 11 (Box 11.3)*, 847-940.

Naud, C. M., J. R. Miller, and C. Landry (2012), Using satellites to investigate the sensitivity of longwave downward radiation to water vapor at high elevations, *J. Geophys. Res.*, *117*, D05101, doi:10.1029/2011JD016917.

Painemal, D., and P. Zuidema (2011), Assessment of MODIS cloud effective radius and optical thickness retrievals over the Southeast Pacific with VOCALS-Rex *in situ*, *J. Geophys. Res.*, *116*, D24206, doi:10.1029/2011JD016155.

Painter, T. J., S. McKensie Skiles, J. S. Deems, A. C. Bryant, and C. C. Landry (2012), Dust radiative forcing in snow of the Upper Colorado River Basin: 1. A 6 year record of energy balance, radiation, and dust concentrations, *Water Resour. Res.*, *48*, W07521, doi:10.1029/2012WR011985.

Platnick, S., M. D. King, S. A. Ackerman, W. P. Menzel, B. A. Baum, J. C. Riédi, and R. A. Frey (2003), The MODIS cloud products: Algorithms and examples from Terra, *IEEE Trans. Geosci. Remote Sens.*, *41*, 459–472.

Rangwala, I. (2012), Amplified water vapor feedback at high altitudes during winter, *Int. J. Climatol.*, doi:10.1002/joc.3477.

Rangwala, I., and J. R. Miller (2009), Warming in the Tibetan Plateau: Possible influences of the changes in surface water vapor, *Geophys. Res. Lett.*, *36*, L06703, doi:10.1029/2009GL037245.

Rangwala, I., and J. R. Miller (2012), Climate change in mountains: A review of elevation-dependent warming and its possible causes, *Clim. Change*, doi:10.1007/s10584-012-0419-3.

Rangwala, I., J. Miller, G. Russell, and M. Xu (2010), Using a global climate model to evaluate the influences of water vapor, snow cover and atmospheric aerosol on warming in the Tibetan Plateau during the twenty-first century, *Climate Dynam.*, *34*(6), 859–872.

Ruckstuhl, C., R. Philipona, J. Morland, and A. Ohmura (2007), Observed relationship between surface specific humidity, integrated water vapor, and longwave downward radiation at different altitudes, *J. Geophys. Res.*, *112*, L19809, doi:10.1029/2005GL023624.

Salomonson, V. V., W. L. Barnes, P. W. Maymon, H. E. Montgomery, and H. Ostrow (1989), MODIS: Advanced facility instrument for studies of the Earth as a system, *IEEE Trans. Geosci. Remote Sens.*, *27*, 145–153.

Stephens, G. L. (2005), Cloud feedbacks in the climate system: A critical review, *J. Climate*, *18*, 237–273.